Int. J. Solids Structures Vol. 27, No. 3, pp. 299–314, 1991
Printed in Great Britain.

0020–7683/91 $3.00 + .00

SPECIAL CASES IN STUDY OF ANOMALOUS DYNAMIC ELASTIC–PLASTIC RESPONSE OF BEAMS BY A SIMPLE MODEL

P. S. SYMONDS
Division of Engineering, Brown University, Providence, RI 02912, U.S.A.

and

FRANCESCO GENNA and ANTONELLA CIULLINI
Department of Structural Engineering, Politecnico di Milano, 20133 Milano, Italy

(*Received* 10 *August* 1989; *in revised form* 5 *December* 1989)

Abstract—Special simplified forms of a single degree of freedom model are used to study anomalous elastic–plastic behavior of fixed-ended beams subjected to short pulse loading. Here the "anomalies" referred to are unexpected sensitivites and counter-intuitive predictions computed for the permanent deflection. The special cases treated are: (1) wholly elastic behavior in the recovery motion, following elastic–plastic deformation in the swing to the first peak deflection; and (2) momentless behavior of the "beam" model, corresponding to vanishing thickness. Used with diagrams of energy changes, these help to clarify the general response and to show the links with some related analyses in the recent literature.

1. INTRODUCTION

The anomalies of interest may be observed in calculated responses for pin-ended or fully fixed beams (Symonds and Yu, 1985; Symonds and Lee, 1989) and edge-fixed plates (Galiev and Nechitailo, 1985) when the transverse pulse of pressure causes moderate plastic deformations. Under these boundary fixing conditions transverse displacements require middle surface extensions. Thus moderate plastic deformations imply change of the beam to a flat arch, and of the plate to a shallow shell. When the total energy available (potential plus kinetic) is sufficient, unstable dynamic states and transitions akin to snap buckling may occur. Hence the final rest equilibrium state may involve the major displacement in the opposite direction to that of the load during the pulse, and other surprising effects may be observed. By means of an energy approach (Borino *et al.*, 1989) a Shanley (single degree of freedom) model has been of great value in investigating these instability phenomena, especially to account for the strong effects of damping. Earlier studies on the undamped structure have also used energy considerations (Reynolds, 1987; Yankelevsky, 1988).

The two special cases considered here serve to illustrate some basic features of the anomalous responses in perhaps the simplest possible manner.

2. PROPERTIES AND EQUATIONS OF THE MODEL

The model consists of two rigid bars connected to each other through a deformable cell, with their opposite ends attached to fixed pins (Fig. 1). The cell is assigned the properties of a sandwich beam whose flanges exhibit linear elastic-perfectly plastic behavior. This enables elastic–plastic beam behavior to be modelled in the presence of geometric non-linearity arising from the fixed end conditions. The parameters of the model are $\mu = E/\sigma_0$ and $\eta = h/l$, where E is the Young's modulus and σ_0 the yield stress of each flange; h is the separation between flanges and $2l$ is the span. The flanges have equal area $A/2$. Note that the model is essentially defined by its equations; various pictorial representations are possible (Symonds and Yu, 1985; Yu and Xu, 1988).

The displacement variable is taken as the angle $\phi(t)$ of rotation (t = time), Fig. 1. For small ϕ, "strain" rates are defined as

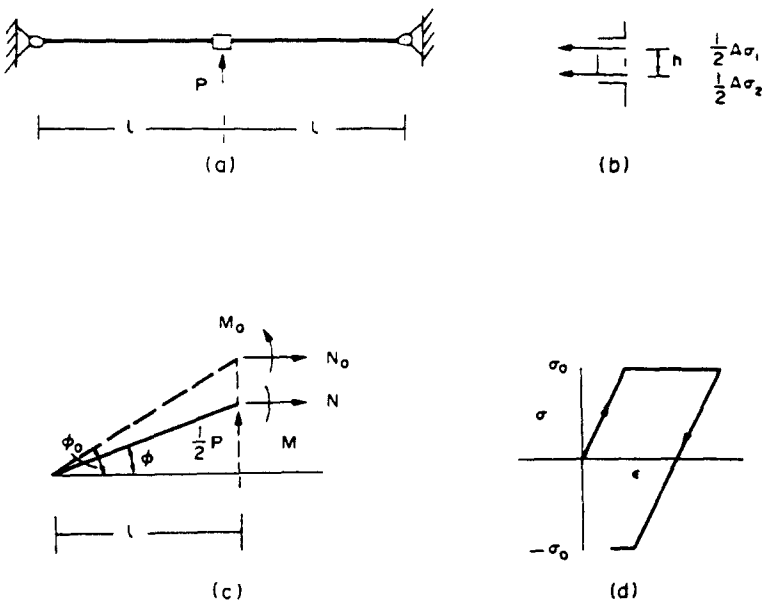

Fig. 1. The Shanley model. (a) indicates rigid bars attached by pins to rigid supports. (b) shows deformable cell with notation for stresses; M, N are bending moment and axial force exerted by cell. (c) shows notation for displacement angle ϕ: peak displacement due to short pulse is ϕ_0, taken as loading parameter. (d) shows elastic–perfectly plastic behaviour assumed for each bar.

$$\dot{\varepsilon}_1 = (\phi + \eta/2)\dot{\phi}; \quad \dot{\varepsilon}_2 = (\phi - \eta/2)\dot{\phi}, \tag{1}$$

where subscripts 1, 2 refer to the upper and lower flanges, respectively, and $\dot{x} = \mathrm{d}x/\mathrm{d}t$. Writing corresponding nondimensional stresses as $s_1 = \sigma_1/\sigma_0$, $s_2 = \sigma_2/\sigma_0$, the strain rates are made up of elastic and plastic components as follows:

$$\dot{\varepsilon}_1 = \dot{s}_1/\mu + \dot{\varepsilon}_1^{\mathrm{p}}; \quad \dot{\varepsilon}_2 = \dot{s}_2/\mu + \dot{\varepsilon}_2^{\mathrm{p}}. \tag{2}$$

The yield and flow rules are

$$\begin{aligned} |s_\alpha| &\leqslant 1 \\ (s_\alpha \pm 1)\dot{\varepsilon}_\alpha^{\mathrm{p}} &\geqslant 0 \\ \dot{s}_\alpha \dot{\varepsilon}_\alpha^{\mathrm{p}} &= 0 \end{aligned} \tag{3}$$

with $\alpha = 1, 2$; no summation over α. Integrating eqns (2),

$$s_1 = \tfrac{1}{2}\mu(\phi^2 + \eta\phi - 2\varepsilon_1^{\mathrm{p}}); \quad s_2 = \tfrac{1}{2}\mu(\phi^2 - \eta\phi - 2\varepsilon_2^{\mathrm{p}}). \tag{4}$$

The equation of motion (angular acceleration) is

$$J\ddot{\phi} + \zeta c_c \dot{\phi} + s_1(\phi + \eta/2) + s_2(\phi - \eta/2) = f(t) \tag{5}$$

where $J = 2ml/3A\sigma_0$, $c_c = (2J\mu\eta^2)^{1/2}$, ζ is the damping ratio, m is the mass of the half-beam, and $f = P(t)/A\sigma_0$ is the dimensionless pulse force. Using expression (4), this takes the form

$$J\ddot{\phi} + \zeta c_c \dot{\phi} + \mu\phi^3 + \mu\alpha\phi + \mu\beta = f(t) \tag{6a}$$

where

$$\alpha = \tfrac{1}{2}\eta^2 - \varepsilon_1^p - \varepsilon_2^p \tag{6b}$$

$$\beta = \tfrac{1}{2}\eta(\varepsilon_2^p - \varepsilon_1^p). \tag{6c}$$

The corresponding work–energy equation ("first integral") is written as

$$V + T = U = U_0 - D_p - D_v + \int_{\phi_0}^{\phi} f \, d\phi \tag{7a}$$

where

$$V = (s_1^2 + s_2^2)/2\mu$$

$$= \tfrac{1}{4}\mu\phi^4 + \tfrac{1}{2}\mu\alpha\phi^2 + \mu\beta\phi + \mu\gamma \tag{7b}$$

$$T = \tfrac{1}{2}J\dot{\phi}^2 \tag{7c}$$

$$D_p = \int_{\phi_0}^{\phi} (s_1 \, d\varepsilon_1^p + s_2 \, d\varepsilon_2^p) \tag{7d}$$

$$D_v = \zeta c_c \int_{\phi_0}^{\phi} \dot{\phi} \, d\phi \tag{7e}$$

$$U_0 = V(\phi_0) + T(\dot{\phi}_0) \tag{7f}$$

$$\gamma = \tfrac{1}{2}[(\varepsilon_1^p)^2 + (\varepsilon_2^p)^2]. \tag{7g}$$

Equations (7) can be derived by integrating eqn (5) with respect to ϕ from the reference value ϕ_0. It states that the total energy U decreases by the amount of plastic work D_p and viscous damping work D_v reckoned from the reference displacement, and increases by the amount of external work, if any.

Note that coefficients α, β, γ depend on the plastic strains ε_1^p, ε_2^p; hence in general are not constant. After plastic deformation has ceased —under short pulse loading the structure will shake down— the coefficients in eqns (6) and (7) are constants. Equation (6a) is then a standard form of Duffing's equation.

The work–energy relation eqn (7a) is a general form for any loading $f(t)$ and reference state ϕ_0, $\dot{\phi}_0$. We take ϕ_0 to be the first peak displacement, with $\dot{\phi}_0 = 0$, and assume this is reached after the pulse force has decreased to zero. Thus ϕ_0 is taken as the single parameter of loading. This makes it unnecessary to consider details of the pulse, and is appropriate since we are here concerned with the final state, not with the maximum deflection *per se*. In other words we are concerned primarily with the "recovery" (initially elastic, but in general elastic–plastic) following the peak displacement ϕ_0. The plastic strains at the peak displacement are assumed to be those resulting from unidirectional displacement from $\phi = 0$ to $\phi = \phi_0$.

This elimination of pulse details from consideration is allowed by the SDoF model, but is not possible in treating the prototype beam/plate problems. There the shapes of the maximum deflection and plastic strain fields will depend on the details of the pulse loading. Unfortunately in the present problem the final state can be extremely sensitive to all the factors that determine the fields of plastic strain and total energy. Results of numerical solutions of eqns (6) and (7) are discussed in what follows, taking $f(t) = 0$ and magnitudes $E/\sigma_0 = \mu = 400$, $J = 6 \times 10^{-8}$ s^2, $\eta = 0.0271$ (except in Section 5 where the momentless case $\eta = 0$ is considered).

3. GENERAL FEATURES OF RESPONSE

Time histories and the final displacements have been obtained by numerical integration of eqn (6) (see Genna and Symonds, 1987, 1988; Borino *et al.*, 1989). (Newmark and central difference schemes have yielded essentially identical results.) The final displacement plotted against the pulse strength parameter ϕ_0 furnishes a "characteristic diagram" for

particular parameters. The example shown in Fig. 2 is for damping coefficient $\zeta = 0.01$ and the model parameters listed in Section 2. The dashed curves show for comparison the envelope of the continuing elastic vibration of the *undamped* structure ($\zeta = 0$). It is seen that the results calculated without damping fail to indicate the signs of the final displacements of the damped model. The diagram for that case shows many narrow intervals ("slots") in which the final displacement is negative, i.e. in the (counter-intuitive) direction opposite that of the loading. A wider slot appears between 0.086 and 0.091 which corresponds roughly to the single band of the undamped model. When the damping coefficient is larger (e.g. $\zeta \geqslant 0.05$) no such correspondence is observed even approximately, and the slots are fewer and wider (Genna and Symonds, 1988).

These are seemingly complex behaviors. In impulsive loading problems one usually ignores damping; we know that the final elastic vibration is damped out, but we can estimate the final deflection quite well from its mean undamped displacement. Here, on the contrary, it seems that one cannot even predict the *sign* of the final rest deflection from calculations made without damping, and the final state depends sensitively on the damping.

These behaviors, which are obtained from many hundreds of displacement–time histories, reflect features of phase plane portraits, such as saddle points and separatrix curves at certain values of the load parameter (see Symonds *et al.*, 1986; Genna and Symonds, 1987, 1988). However in the present class of problems where small plastic deformations play a critical role, phase plane diagrams are not very helpful because they indicate these effects only indirectly. Much more help in understanding the present phenomena is obtained from an energetic approach (Borino *et al.*, 1989; Perego *et al.*, 1989). This involves a simple idea, but apparently not previously utilized, namely that of plotting together the *elastic strain energy* V (i.e. the potential energy) and the *total available energy* U (i.e. the sum of

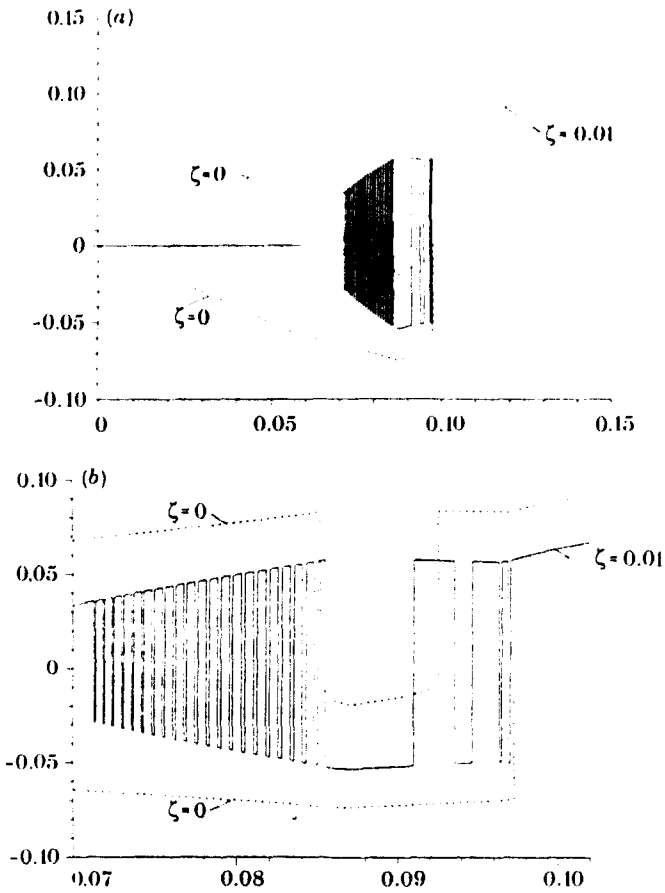

Fig. 2. Final displacement as function of initial displacement angle, for damping ratio $\zeta = 0.01$ [from Genna and Symonds (1988)]. Dashed curves show envelope of final elastic vibration for case of zero damping. (b) shows expanded scales.

the kinetic and strain energies), both as functions of the displacement variable. Examples of these plots are given in Fig. 3, where V is plotted with solid lines and U with dashed lines. We review these results briefly here, as a preliminary to considering the special cases of main interest in this paper.

Each diagram in Fig. 3 contains two continuous curves, each with many branches. They start together at point O. They meet again at points where the kinetic energy vanishes, which mark the successive extrema of the deflection. The U curve decreases smoothly because of energy loss in damping, but shows abrupt drops when plastic dissipation occurs. Eventually plastic deformation ceases, and the zig-zag pattern of the U curve depicts the final elastic vibration, whose amplitude decreases in successive cycles. The V curve shows abrupt changes in slope at points where plastic strain increments occur. These are marked as points A_1 and A_2 on both curves, in the traverse from O to B.

In the present single degree of freedom model it is found (empirically; it is not true in general) that plastic flow occurs *only* in the first swing from the starting point O to the first minimum deflection, marked as B. Thus the first swing is depicted in Figs 3 by the curves

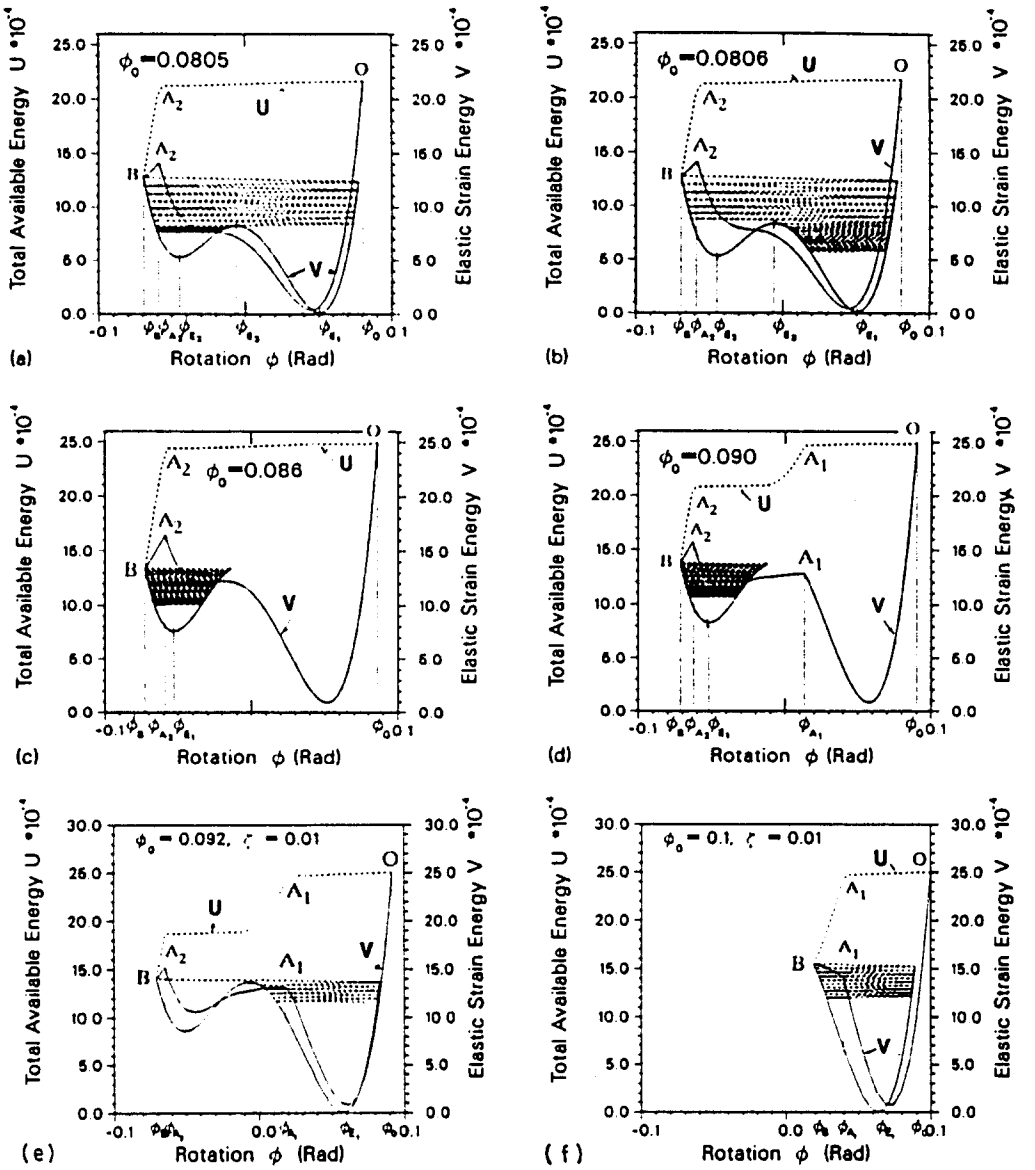

Fig. 3. Energy diagrams for damping ratio $\zeta = 0.01$. Solid lines show the strain energy $V(\phi; \phi_0)$, dashed lines show the total energy $U(\phi; \phi_0)$.

O–A_2–B in (a), (b), (c), by the curves O–A_1–A_2–B in (d), (e), and by curves O–A_1–B in (f). Since the motion after reaching point B is wholly elastic, the strain energy curve thereafter has constant shape (a quartic function with constant coefficients). The state point traverses it to successive peaks, as the amplitude decreases asymptotically to zero. The final state is at one or the other of the two local minima of the V curve.

The character of the response depends on the shape of the final V (strain energy) curve. In the examples of Fig. 3 there is a "potential hill" with crest at a small negative displacement. This is a position of unstable equilibrium, lying between two stable equilibria at the local minima. The final V curve is governed by the prior plastic straining. This in turn is affected by the damping. The U curve descends until one of its branches meets the potential hill. It is then "reflected", and for the rest of the response, it remains on the same side as the original contact point. Which side it first strikes depends sensitively on the damping coefficient and on the initial displacement. The origin of the "slots" of Fig. 2 is apparent.

These illustrations show how the combined energy plots "open up" the response process, showing how the interplay between geometry changes, dynamics and energy losses determines the final outcome. They must be obtained by numerical integration. There is instructive value in considering two special cases that are simpler and allow further insight. These are treated in the following sections.

4. ELASTIC RECOVERY

In the examples discussed above, the structure model is assumed to have the same elastic–plastic material behaviors throughout the response. Important plastic strains actually occur in the recovery motion, as well as in the preceding displacement. Here we shall assume arbitrarily that the recovery motion is entirely elastic. In effect we put $\sigma_0 \to \infty$ for time subsequent to reaching the peak displacement ϕ_0.

The plastic strains ε^p_{10}, ε^p_{20} at angle ϕ_0, acquired after unidirectional displacement, are

$$\varepsilon^p_{10} = \left[\frac{1}{2}(\phi_0^2 + \eta\phi_0) - \frac{1}{\mu}\right] H(\phi_0 - \phi_0^{(1)}) \tag{8a}$$

$$\varepsilon^p_{20} = \left[\frac{1}{2}(\phi_0^2 - \eta\phi_0) - \frac{1}{\mu}\right] H(\phi_0 - \phi_0^{(2)}) \tag{8b}$$

where

$$H(F) = 1 \quad \text{for} \quad F \geqslant 0$$
$$H(F) = 0 \quad \text{for} \quad F < 0,$$

for $\eta = 0.0271$: $\phi_0^{(1)} = 0.058447$, $\phi_0^{(2)} = 0.085547$.

With ε^p_{10}, ε^p_{20} inserted for ε^p_1 and ε^p_2 in eqns (6) and (7), all coefficients in eqns (6a) and (7a) are constant.

Although "elastic recovery" is apparently an artificial concept, the behavior does represent essential features of the prototype uniform beam problem. In the real problem the pulse loading produces fields of plastic strain and specific total energy. In order to predict the final rest configuration, one must know both of these fields. They require step-by-step numerical integration, and hence are never known "exactly". When elastic recovery is postulated these fields can be regarded as known parameters. Study of this case is a simple way to show many of the general features of the complex uniform beam problem, excluding possible difficulties associated with numerical computations of plastic strains. Also, of course, comparisons with solutions for the elastic–plastic case enable one to assess the role of the actual further plastic deformations subsequent to the peak deflection.

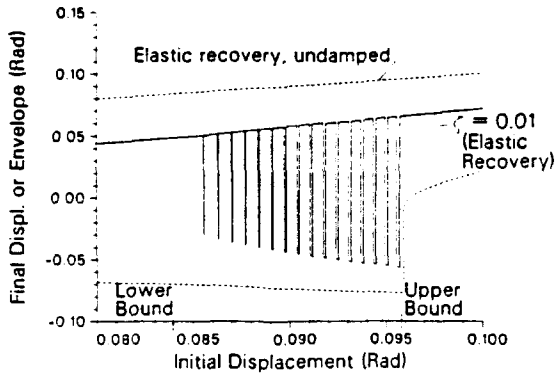

Fig. 4. Elastic recovery case: final displacement as function of the starting angle, for damping ratio $\zeta = 0.01$. Dashed lines show envelope of final vibration for the undamped, elastic recovery case.

A characteristic diagram for the elastic recovery case is shown in Fig. 4. This shows the final displacement as a function of ϕ_0 for damping ratio $\zeta = 0.01$. There are 16 narrow "slots" with negative values. Also shown for comparison (dashed lines) are the envelope curves for the elastic vibration in the undamped case. Note that when damping is omitted there is no indication that negative final displacements will occur; the vibration switches from a $(+)$-$(-)$ to a $(+)$-$(+)$ type at ϕ_0 about 0.096, but there is no range in which the envelope is wholly negative. In contrast, the final displacement of the damped motion is frequently negative for ϕ_0 in the range between about 0.085 and 0.096.

This alternation between positive and negative final displacements can be predicted immediately from the energy diagrams already discussed. These make it clear that if the strain energy curve $V(\phi; \phi_0)$ has two distinct relative minima separated by a "potential hill", the final state will oscillate between the two stable equilibrium positions as the initial displacement is varied. Unlike the examples of Fig. 3, the function $V(\phi; \phi_0)$ of eqn (7b) can be plotted at once without the need for numerical integration of eqn (6a), since the plastic strains $\varepsilon^p_{10}, \varepsilon^p_{20}$ are known in terms of ϕ_0 [eqns (8)]. Figure 5 shows $V(\phi)$ for a typical case, $\phi_0 = 0.09$. This figure also shows the curves of total energy $U(\phi)$ for three values of damping ratio ζ. When $\zeta = 0$, U stays constant at the initial value U_0. [By eqn (7b), $U_0 = V_0 = (1+1)/2\mu = 25 \times 10^{-4}$.] Curves for two nonzero values of ζ are included. These show U decreasing in zig-zag fashion until the curve strikes and is reflected from the potential hill. The value of ζ_1 is such that contact is made on the left-hand side. Thereafter the vibration remains on this side, and the negative static equilibrium position ϕ_{E2} is finally reached. With a small decrease of ζ to ζ_2, the contact point switches to the right-hand side of the hill, and the final state is on the positive side.

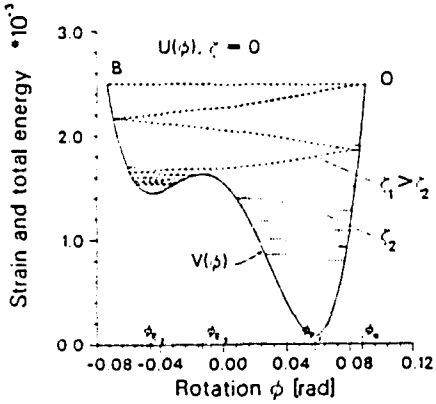

Fig. 5. Elastic recovery case: strain energy $V(\phi; \phi_0)$ for $\phi_0 = 0.09$ (solid curve); total energy $U(\phi; \phi_0)$ curves for two slightly different damping ratios ζ_1 and ζ_2 (dotted and dashed, respectively).

When ϕ_0 is gradually increased, with ζ held constant, the alternation in final displacement occurs because the crest of the potential hill rises relative to the $V(\phi;\phi_0)$ curve. The process is the same as that depicted in Figs 3a and 3b, the only difference being that in the elastic recovery case, the $V(\phi;\phi_0)$ curve is computed from the plastic strains postulated at the start, rather than computed by step-by-step integration.

Prediction of the final displacement for any specified values of ϕ_0 and ζ requires step-by-step integration of eqn 6a. This is straightforward unless ζ is very small, as far as the mathematical problem is concerned. The range of ϕ_0 in which the anomalous "slots" occur can be estimated, however, making use only of properties of the $V(\phi;\phi_0)$ curve. This has been done for the elastic–plastic case (Borino *et al.*, 1989). It is much easier when elastic recovery is assumed, and is worth briefly sketching.

A negative final displacement can occur only if the $V(\phi;\phi_0)$ curve exhibits the general shape of the typical case drawn in Fig. 5. There must be three distinct real roots of the equation for static equilibrium $\mathrm{d}V/\mathrm{d}\phi = 0$, hence of the equation

$$\phi^3+\alpha\phi+\beta = 0 \tag{9a}$$

where

$$\alpha = \tfrac{1}{2}(\eta^2-\phi_0^2-\eta\phi_0+2/\mu) \tag{9b}$$

$$\beta = -\tfrac{1}{2}\eta(\phi_0^2+\eta\phi_0-2/\mu). \tag{9c}$$

These are for $\varepsilon_{10}^p \neq 0$, $\varepsilon_{20}^p = 0$. A lower bound on ϕ_0 for anomalous final displacements is provided by the well known condition for coalescence of real roots of a cubic equation. In the present case this condition requires

$$\frac{1}{27}\alpha^3+\frac{1}{4}\beta^2 = 0, \tag{10}$$

where α, β are functions of ϕ_0 as in eqn (9). Solutions of eqn (10) provide a lower bound ϕ_0^L.

At large values of ϕ_0 the crest at ϕ_{E3} of the potential hill lies above the starting value $V(\phi_0;\phi_0)$. The response is then always on the positive side of the hill. The limiting condition is expressed by the equations

$$V(\phi_{E3};\phi_0) = V(\phi_0;\phi_0) \tag{11a}$$

$$V'(\phi_{E3};\phi_0) = 0, \tag{11b}$$

where $V' = \mathrm{d}V/\mathrm{d}\phi$.

Now α and β correspond to $\varepsilon_{10}^p \neq 0$, $\varepsilon_{20}^p \neq 0$, and are expressed by

$$\alpha = \tfrac{1}{2}(\eta^2-2\phi_0^2-4/\mu) \tag{11c}$$

$$\beta = -\tfrac{1}{2}\eta^2\phi_0. \tag{11d}$$

Solutions of eqn (11) provide an upper bound ϕ_0^U for $\eta = 0.0271$, $\phi_0^L = 0.083984$, $\phi_0^U = 0.095887$. The limiting $V(\phi;\phi_0)$ curves are drawn in Fig. 6 (solid lines).

5. MOMENTLESS BEAM MODEL

We consider next the special case of a model that has no flexural resistance, by taking the parameter $\eta = h/l = 0$. Thus, the two flanges of the sandwich beam reduce to a single thin flange of area A, which has strain ε and dimensionless stress $s = \sigma/\sigma_0$. In addition to the basic eqns (3), where $s_x = s$, we have

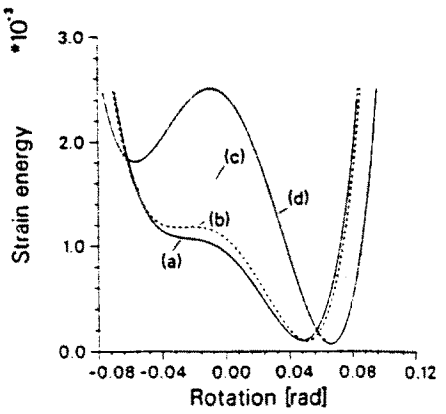

Fig. 6. Elastic recovery case: strain energy $V(\phi;\phi_0)$ for different starting angles. (a) $\phi_0 = \phi_0^c = 0.083984$; (b) $\phi_0 = 0.085547$ (elastic limit for the bottom bar, i.e. $\varepsilon_0^p > 0$ for $\phi_0 > 0.085547$); (c) $\phi_0 = 0.09$ (typical); (d) $\phi_0 = \phi_0^c = 0.095887$.

$$\varepsilon = \phi^2/2; \quad s = \mu(\phi^2/2 - \varepsilon^p) \tag{12a,b}$$

$$J\ddot{\phi} + \zeta c_c \dot{\phi} + \mu\phi^3 - 2\mu\varepsilon^p\phi = f(t). \tag{13}$$

[The damping coefficient may still be written in terms of a damping ratio ζ and critical damping coefficient c_c defined as before for a model with nonzero η; numerical values of ζ refer to c_c computed from the previously listed values of J, μ, η; see eqn (6).] As before, we assume that the pulse produces a peak displacement ϕ_0 which is taken as the loading parameter. The corresponding stress and plastic strain state are assumed produced by unidirectional displacement. We put $f(t) = 0$ during the subsequent recovery motion.

With $\eta = 0$ it is found that plastic flow occurs only during the first swing to the peak angle ϕ_0. Thereafter the plastic strain remains constant at the value ε_0^p reached when $\phi = \phi_0$ and $s = 1$, namely

$$\varepsilon_0^p = \frac{1}{2}\phi_0^2 - \frac{1}{\mu}. \tag{14}$$

Thus the threshold for plastic deformation is $\phi_0^c = (2/\mu)^{1/2}$. The energy relation eqn (8) now involves the strain energy V with $\varepsilon^p = \varepsilon_0^p$ so that

$$V(\phi;\phi_0) = \mu\left(\frac{1}{2}\phi^2 - \varepsilon_0^p\right)^2 = \mu\left(\frac{1}{2}\phi^2 - \frac{1}{2}\phi_0^2 + \frac{1}{\mu}\right)^2. \tag{15}$$

The positions of stable static equilibrium (local minima) are

$$\phi_E = \pm(2\varepsilon_0^p)^{1/2} = \pm(\phi_0^2 - 2/\mu)^{1/2}. \tag{16}$$

The diagram is now symmetric in ϕ, and the crest of the potential hill at $\phi = 0$ is at

$$V(0;\phi_0) = \mu(\varepsilon_0^p)^2 = \tfrac{1}{4}\mu(\phi_0^2 - 2/\mu)^2. \tag{17}$$

The full range of dynamic behavior can be deduced from the $V(\phi;\phi_0)$ diagram. Figure 7

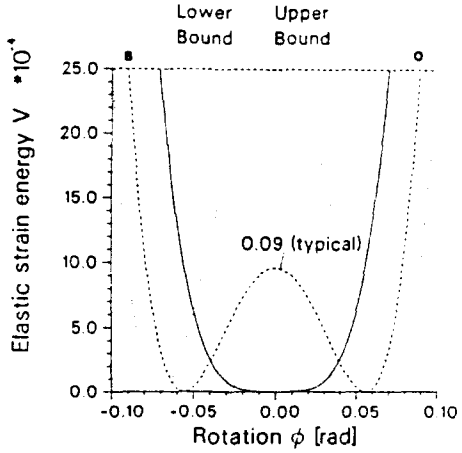

Fig. 7. Momentless (thin) beam case: strain energy $V(\phi;\phi_0)$ for different starting angle values: solid curve, $\phi_0 = \phi_c = 0.070710678$; dashed curve $\phi_0 = 0.09$ (typical); dotted curve, $\phi_0 = \phi_0^t = 0.10$.

shows $V(\phi;\phi_0)$ for several values of ϕ_0, at or above the elastic limit $\phi_0^c = 0.07071$. Consider as a "typical" case $\phi_0 = 0.09$. Motion starts at point 0, where $U(\phi_0;\phi_0) = V(\phi_0;\phi_0) = 1/\mu = 25 \times 10^{-4}$. Suppose first that damping is zero. Then the total energy $U(\phi;\phi_0)$ remains at this value, while the state point traverses the $V(\phi;\phi_0)$ curve between 0 and B; the vibration continues indefinitely between these limits. The kinetic energy is represented by the distance from the line OB to the $V(\phi;\phi_0)$ curve, and the phase plane diagram has an hour glass shape (as in Fig. 10b), symmetric about the ϕ and $\dot{\phi}$ axes. As ϕ_0 is increased, the value $V(0;\phi_0)$ eventually reaches the starting value $V(\phi_0;\phi_0)$. By eqn (17) this happens at $\phi_0^t = (4/\mu)^{1/2} = 0.1$. At larger values of ϕ_0, the potential hill extends above the line for $U = U_0$, and the vibration remains on the positive side.

When damping is included ($\zeta > 0$), the final state is at one of the two stable equilibrium points $\phi = \pm(2\varepsilon_0^c)^{1/2}$, eqn (16). Which of the two is reached depends sensitively on ζ and ϕ_0. From the discussion in the previous sections, it is obvious that the final displacement will alternate in sign either as ζ is increased, with ϕ_0 constant; or as ϕ_0 is increased, at constant ζ. A negative final displacement can occur when ϕ_0 exceeds the elastic limit $\phi_0^c = (2/\mu)^{1/2}$, which is a lower bound, so that

$$\phi_0^c = \phi_0^t = (2/\mu)^{1/2} \leqslant \phi_0 \leqslant \phi_0^t = (4/\mu)^{1/2}. \tag{18}$$

The characteristc diagrams for $\zeta = 0$ and $\zeta = 0.06$ are shown in Fig. 8, from data

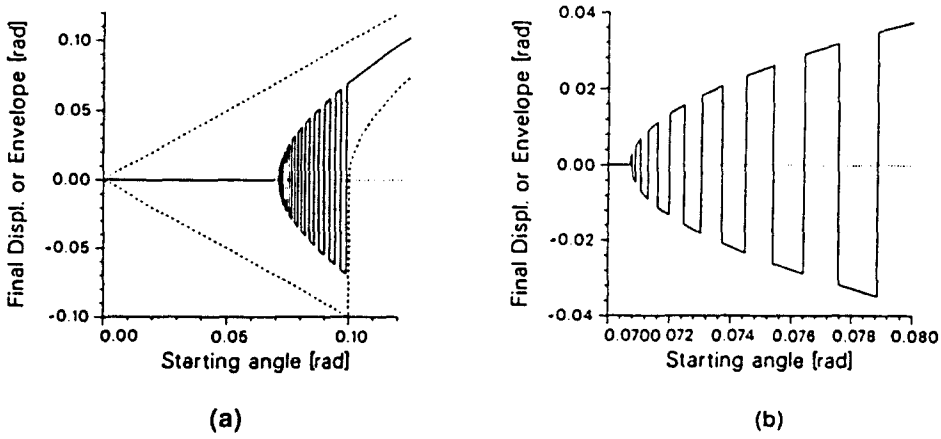

Fig. 8. Thin beam case: characteristic diagram for damping ratio $\zeta = 0.06$; dashed lines show envelope of the final vibration for the undamped, $\eta = 0$ case. (a) and (b) show differently expanded scales.

obtained by numerical integration of eqn (13). These agree with the descriptions outlined above. However, the pattern of "slots" exhibited by the curve for the final displacements of the damped model differs in important respects from those of Figs 2 and 4. The lower bound on their appearance is the elastic limit ϕ_0^e, and the calculations indicate that as ϕ_0^e is approached from above they become extremely narrow and difficult to identify. This difficulty can be understood by inspection of the energy diagrams of Figs 9a, 9b. As indicated in Fig. 9a (for $\phi_0 = \phi_0^e$), the beam executes infinitely many oscillations during its asymptotic approach to the final rest state at $\phi = 0$. As ϕ_0 is increased slightly above ϕ_0^e, as in Fig. 9b, the descending branches of the $U(\phi\,;\phi_0)$ curve are reflected in turn from alternate sides of the potential hill of the $V(\phi\,;\phi_0)$ curve as it rises. These branches change slightly as ϕ_0 is increased, but if this is ignored, the alternation of the final state between the values $\pm(2\varepsilon_0^p)^{1/2}$ can be visualized as cutting successive branches of the $U(\phi\,;\phi_0)$ curve for $\phi_0 = \phi_0^e$. Any finite rise from zero of the hill implies in the present case cutting an infinite number of infinitely close branches. Computing all the slots in this case is not merely difficult but impossible, since the width of the slot vanishes as ϕ_0^e is approached. This is in contrast with the elastic recovery case treated above, where for finite ζ the first slot encountered as ϕ_0 is increased has finite width. Difficulty in locating its boundaries is encountered only if ζ is extremely small. In the momentless beam case, however, the difficulty is present whatever the damping magnitude. The basic difference is the symmetry of the $V(\phi\,;\phi_0)$ curve.

To apply these ideas in quantitative terms, we derive an approximate expression for the widths of the slots shown in Fig. 8. Assuming that the $U(\phi\,;\phi_0)$ curve changes negligibly as ϕ_0 is increased, the width of a slot is approximately equal to the increment $\Delta\phi_0$ such that the increase in $V(0\,;\phi_0)$ corresponding to $\Delta\phi_0$ is equal to the energy loss in damping in one half-cycle. In order to estimate the latter, we shall assume that an approximate expression for the velocity can be used which satisfies the main requirements of energy conservation. Thus, to make our estimate we assume that

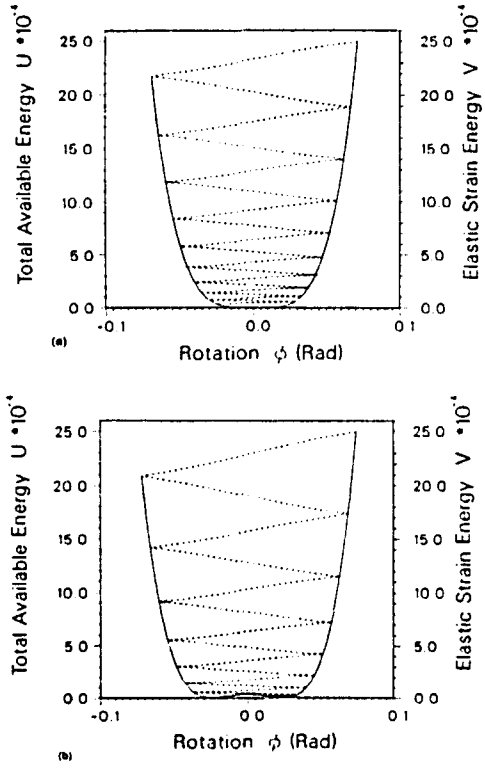

Fig. 9. (a) Thin beam case: strain energy $V(\phi\,;\phi_0)$ (solid) and total energy $U(\phi\,;\phi_0)$ (dashed) for $\phi_0 = \phi_r = 0.070710678$. Damping ratio $\zeta = 0.06$. (b) Thin beam case: strain energy $V(\phi\,;\phi_0)$ (solid) and total energy $U(\phi\,;\phi_0)$ (dashed) for $\phi_0 = 0.075$. Damping ratio $\zeta = 0.06$.

$$\frac{\partial V(0;\phi_0)}{\partial \phi_0}\Delta\phi_0 \cong \zeta c_c \int_{-\phi_m}^{\phi_m} \dot{\phi}\, d\phi, \tag{19}$$

where ϕ_m is the deflection amplitude. Note that

$$2(\varepsilon_0^p)^{1/2} \leqslant \phi_m \leqslant \phi_0 \tag{20}$$

since the amplitude decreases from ϕ_0 to the value such $V(\phi_m;\phi_0) = V(0;\phi_0)$; by eqn (15), $\phi_m \geqslant 2(\varepsilon_0^p)^{1/2}$. To obtain $\dot{\phi}$ in eqn (18) we write the following approximation for $\phi(t)$:

$$\phi(t) = \phi_m[\alpha \cos pt + (1-\alpha)\cos 3pt] \tag{21a}$$

$$\dot{\phi}(t) = -p\phi_m[\alpha \sin pt + 3(1-\alpha)\sin 3pt], \tag{21b}$$

where for a typical half-cycle the argument $pt \in [0, \pi]$ corresponds to $\phi \in [\phi_m, -\phi_m]$, neglecting the decrease in amplitude due to damping in the half-cycle. We obtain reasonable values of α and p by matching known kinetic energies in the undamped case at $pt = \pi/2$ and pt_c, where $\dot{\phi}$ has minimum and maximum values, respectively, for $p\tau \in (0, \pi)$.

The results are

$$\sin pt_c = \left[\frac{9-8\alpha}{36(1-\alpha)}\right]^{1/2} \tag{22a}$$

$$(pt = pt_c): \qquad p^2 = \frac{162(1-\alpha)}{(9-8\alpha)^3}\frac{\mu}{J\phi_m^2}\left[\frac{\phi_m^2}{2} - \varepsilon_0^p\right] \tag{22b}$$

$$(pt = \pi/2): \quad \tfrac{1}{2}Jp^2(4\alpha-3)^2\phi_m^2 = \tfrac{1}{4}\mu\phi_m^2(\phi_m^2 - 4\varepsilon_0^p). \tag{22c}$$

Eliminating p between the last two, a general relation between α, ϕ_0 and ϕ_m is

$$\frac{(9-8\alpha)^3}{81(1-\alpha)(4\alpha-3)^2} - 1 = \frac{4(\varepsilon_0^p)^2}{\phi_m^2(\phi_m^2 - 4\varepsilon_0^p)}. \tag{23}$$

Taking $\phi_m = 2(\varepsilon_0^p)^{1/2}$, we obtain

$$\alpha = \frac{3}{4}; \quad p^2 = \frac{3}{8}\frac{\mu}{J}\varepsilon_0^p \tag{24a,b}$$

$$\Delta\phi_0 = \frac{9\pi}{8}\frac{\zeta c_c}{\phi_0}\left[\frac{3\varepsilon_0^p}{8\mu J}\right]^{1/2} = 0.083\frac{\zeta}{\phi_0}\left[\frac{1}{2}\phi_0^2 - \frac{1}{\mu}\right]^{1/2}. \tag{25a}$$

For $\zeta = 0.06$ in our example we have

$$\Delta\phi_0 = 0.00352\left[1 - \frac{2}{\mu\phi_0^2}\right]^{1/2}. \tag{25b}$$

These results, eqns (25), show the slot width vanishing both as ζ approaches zero and as ϕ_0 approaches $(2/\mu)^{1/2}$, the elastic limit. In either case the final deflection becomes difficult or impossible to compute. In the previous cases with $\eta > 0$, the final response becomes unpredictable in the limit as $\varepsilon \to 0$, $0 < \zeta < \varepsilon$. The present case involves a new type of computational unpredictability, not requiring ζ to be small.

The magnitudes predicted by eqn (25b) have been compared with those according to the data for Fig. 8. The coefficient 0.00352 is too large. If it is replaced by 0.00268 it gives an excellent fit for the first 10 slots. The assumptions underlying these results are probably

more accurate at smaller ζ values. The approximate vibration frequency given by eqn (22b) has been compared with exact values, expressed in terms of an elliptic integral. Putting $\phi_m = \phi_0$ and solving eqn (23) for α, the result for p is very close to the exact value except near the transition point $\phi_0 = (4/\mu)^{1/2}$, where it gives a finite magnitude instead of zero.

To show relations to other work we may adopt a different point of view. Up to now we have considered the "impact problem", namely that of finding the final displacement of a straight beam that is subjected to a short pulse loading. We now consider the behavior of the initially deformed beam, i.e. of a shallow arch, which is subjected to various further loads. Its shape is defined by the plastic strain ε_0^p due to the original pulse loading. We take its "natural" state to be the positive equilibrium position $\phi_E = (2\varepsilon_0^p)^{1/2}$. It is convenient to write $y = \phi/\phi_E = \phi/(2\varepsilon_0^p)^{1/2}$. The equation of motion is

$$J\phi_E\ddot{y} + \zeta c_c \phi_E \dot{y} + \mu\phi_E^3 y^3 - \mu\phi_E^3 y = g(t). \tag{26a}$$

This can be re-written as

$$\ddot{y} + \gamma\dot{y} + \tfrac{1}{2}y^3 - \tfrac{1}{2}y = F(\tau), \tag{26b}$$

writing $\dot{y} = \mathrm{d}y/\mathrm{d}\tau$, replacing the physical time t by a dimensionless time τ, where

$$\tau = t(2\mu\phi_E^2/J)^{1/2}.$$

The energy equation corresponding to eqn (26b) is written as follows in terms of "initial" values y_0, $\dot{y}_0$.

$$T + V = U = T_0 + V_0 - \gamma\int_{y_0}^{y}\dot{y}\,\mathrm{d}y + \int_{y_0}^{y}F\,\mathrm{d}y \tag{27a}$$

where

$$T(\dot{y}) = \tfrac{1}{2}\dot{y}^2; \quad V(y) = \tfrac{1}{8}(y^2-1)^2$$
$$T_0 = T(\dot{y}_0); \quad V_0 = V(y_0). \tag{27b,c}$$

The behavior of the system governed by eqn (26b) was studied by Dowell and Pezeshki (1986); see also Dowell (1988). They carried out numerical integrations to obtain time histories, phase plane plots and Poincaré maps for excitation defined either by initial conditions with $g(\tau) = 0$, or by external sinsusoidal forcing $F = F_0 \sin\omega\tau$. In the first ("autonomous") case, phase plane diagrams were constructed which show the zones within which the initial conditions lead to trajectories which cross the $y = 0$ axis 0, 1, 2... times (termed "shell plots" from their appearance). The trajectories that bound the lowest zones appear to have significance in connection with the onset of chaos, as explored in their investigation of the sinusoidally forced system.

Here we do not add materially to the results of Dowell and Pezeshki's (1986) study. However, the new energy plots do perhaps make the shell diagrams and their significance intuitively more transparent. From sketches of U and V the main features of both the undamped and damped autonomous response can be quickly recognized qualitatively and calculated approximately.

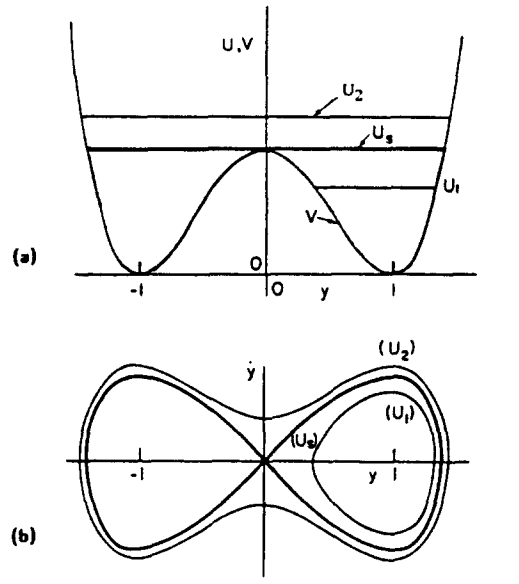

Fig. 10. Plastically strained thin beam with zero damping. Relation between energy diagrams (a) and phase plane diagrams (b). Heavy line at total energy level U_s corresponds to separatrix curve in phase plane. V is elastic strain energy, y is displacement variable. Shaded area in energy diagram indicates locus of energy levels such that motion remains on one side or the other of the axis $y = 0$.

The undamped case is illustrated in Fig. 10, where Fig. 10a shows the energy plots. Here the total energy U is constant at its initial value, and the corresponding horizontal lines are drawn for three values. The middle one of these with $U = U_s$ corresponds to the separatrix in the phase plane diagram, Fig. 10b. At a smaller value $U_1 < U_s$ the vibration lies between positive displacement limits, while for the case $U_2 > U_s$ it lies between equal positive and negative values.

Figure 11 illustrates the behavior when damping is present. Suppose the motion is started from rest at O_1. The dashed line shows approximately how the curve of total energy

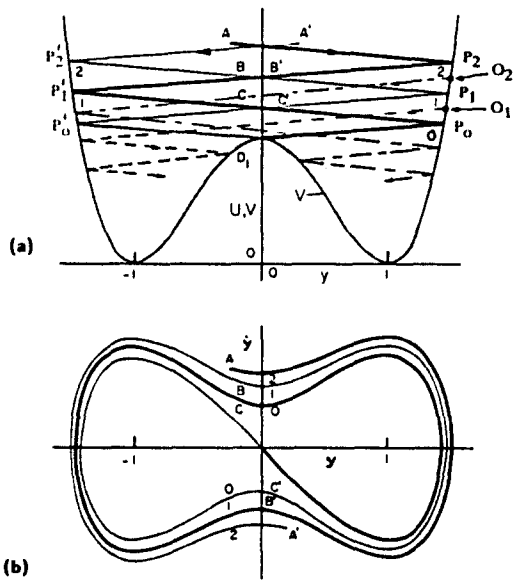

Fig. 11. Plastically strained thin beam with damping. Relation between energy diagrams (a) and phase plane diagrams (b). Straight lines in (a) are crude representation of total energy variation as functions of displacement y. Corresponding phase plane curves are shown in (b). Shaded area in (a) indicates locus of initial energy such that the resulting motion remains on one side of the axis $y = 0$.

U descends as energy is dissipated in damping. In each branch the curve is drawn crudely as a straight line, representing the average slope of the actual curve whose slope varies from zero at each end to maximum values near the equilibrium points $y = \pm 1$. The curve starting from O_1 strikes the potential hill at D_1 and leads finally to the equilibrium point $y = -1$. On the other hand, a starting point at O_2 leads (dot–dash curve) to contact with the right-hand side and finally to equilibrium at $y = +1$.

Also drawn in Fig. 11a are two curves (solid lines), each with several branches. One branch in each curve just touches the potential hill. These also are sketched crudely as straight lines. The actual curves would make contact at the center (at zero slope), instead of slightly to one side, but this discrepancy is unimportant for present purposes. Pairs of these curves mark the boundaries of zones of starting conditions such that the final state is either $+1$ or -1. For example, a motion started from rest at any point between P_1 and P_2 ends up at $y = 1$. From these curves, with account taken of the signs of the velocity, one can readily sketch the corresponding contours in the y, $\dot{y}$ (phase) plane, i.e. the "shell plots" of Dowell and Pezeshki (1986). Figure 11b shows sketches of the first few zones of a typical shell diagram. Note that the shaded area of Fig. 11a defines the locus of energies such that no crossing of the $y = 0$ axis takes place. The $U(y)$, $V(y)$ energy plots are essentially equivalent to the y, $\dot{y}$ phase plane plots, but are perhaps simpler and closer to the basic mechanics. They may help to understand the seemingly more complex phase plane diagrams. For example, they make it obvious that the shell diagram consists of two distinct interleaved curves.

To illustrate how the two types of plots may be used together, we note that the width Δy_0 of the first zone of the shell diagram computed by Dowell and Pezeshki (1986) can be estimated by the approximate approach used in the previous section to estimate the slot widths of the original "impact problem". By inspection of Fig. 11b it is seen that

$$\Delta V \cong \frac{\partial V(y_0)}{\partial y_0} \Delta y_0 = \gamma \int_{y_0}^{y_0} \dot{y}\, dy. \tag{28}$$

Evaluating the RHS approximately by the same process as was used following eqn (19), we obtain

$$\Delta y_0 = \gamma \frac{9}{8} \pi \left(\frac{3}{16}\right)^{1/2} = 0.026. \tag{29}$$

Here we have put $\gamma = 0.0168$ as used by Dowell and Pezeshki (1986); the result agrees well with the spacing shown in their Fig. 2.

6. CONCLUSIONS

These examples are meant to illustrate as simply as possible how the geometry changes due to plastic straining interact with energy transfers and losses to control the approach to the final deformed state. In these nonlinear problems, where small plastic deformations may play a crucial role, the new energy plots show *directly* the occurrence of plastic strain increments, and their effect on the evolving response. In contrast, phase plane diagrams give only indirect evidence of these interactions, and by themselves in the present problems they are of little use.

The energy concepts provide insight into the nature of the solutions. For example, the initial conditions that lead to certain final displacements may be plotted as points in a plane where the axes are the initial displacement and velocity. There are well-defined bands within which the initial conditions lead to a negative final displacement. Elsewhere they result in a non-negative final state. These bands depend strongly on the damping coefficient. Examples are given by Perego *et al.* (1989). Consideration of the energy diagrams with damping shows at once why the boundaries between these "attracting basins" are smooth curves that in general can be calculated accurately by standard methods. The exceptional situations

(very small damping and vanishing bending resistance) are elucidated by the energy diagrams of the "special cases" discussed here. Contrary to the implications of a recent paper (Poddar *et al.*, 1988) these boundaries have no fractal structure (see Symonds *et al.*, 1988).

Acknowledgement—Support from the U.S. Army Research Office under Contract DAAL03-87-K-0038 is gratefully acknowledged.

REFERENCES

Borino, G., Perego, U. and Symonds, P. S. (1989). An energy approach to anomalous damped elastic-plastic response to short pulse loading. *ASME J. Appl. Mech.* **56**, 430–438.

Dowell, E. H. (1988). Chaotic oscillations in mechanical systems. *Computational Mech.* **3**, 199–216.

Dowell, E. H. and Pezeshki, C. (1986). On the understanding of chaos in Duffing's equation including a comparison with experiment. *ASME J. Appl. Mech.* **53**, 5–9.

Galiev, Sh. U. and Nechitailo, N. V. (1985). *The dynamics of forming of thin plates into shells of revolution.* Preprint of the Institute of Problems of Strength, Academy of Sciences of the Ukranian SSR, Kiev, U.S.S.R. (in Russian).

Genna, F. and Symonds, P. S. (1987). Induced vibrations and dynamic plastic instabilities of a nonlinear structural model due to pulse loading. *Meccanica* **22**, 144–149.

Genna, F. and Symonds, P. S. (1988). Dynamic plastic instabilities in response to short pulse excitation—effects of slenderness ratio and damping. *Proc. R. Soc. Lond.* **A417**, 31–44.

Perego, U., Borino, G. and Symonds, P. S. (1989). The role of damping in anomalous response to short pulse loading. *Proc. ASCE J. Engng Mech.* **115**(12), 2782–2788.

Poddar, B., Moon, F. C. and Mukherjee, S. (1988). Chaotic motion of an elastic-plastic beam. *ASME J. Appl. Mech.* **55**(1), 185–189.

Reynolds, D. (1987). The counter-intuitive response of an elastic plastic beam under impulse loading. Report, Department of Mechanical Engineering, University College Galway, Galway, Ireland.

Symonds, P. S., Borino, G. and Perego, U. (1988). Chaotic motion of an elastic-plastic beam. *ASME J. Appl. Mech.* **55**(3), 745–746. [Discussion of paper by Poddar, B., Moon, F. C. and Mukherjee, S. Vol. **55**(1), 185–189.]

Symonds, P. S. and Lee, Jae-yeong (1989). Anomalous and unpredictable response to short pulse loading. In *Recent Advances in Impact Dynamics of Engineering Structures* (Edited by D. Hui and N. Jones), AMD-Vol. 105, AD-Vol. 17, pp. 31–38. ASME, New York.

Symonds, P. S., McNamara, J. F. and Genna, F. (1986). Vibrations and permanent displacements of a pin-ended beam deformed plastically by short pulse excitation. *Int. J. Impact Engng* **4**, 72–82.

Symonds, P. S. and Yu, T. X. (1985). Counterintuitive behavior in a problem of elastic plastic beam dynamics. *ASME J. Appl. Mech.* **52**, 517–522.

Yankelevsky, D. Z. (1988). Vibrations of a pin-ended beam located by a short pulse. *Int. J. Impact Engng* **7**, 345–356.

Yu, T. X. and Xu, Y. (1989). The anomalous response of an elastic plastic structural model to impulsive loading. *ASME J. Appl. Mech.* **56**, 868–873.